Journal of Orthopaedic Translation 24 (2020) 76–87

Contents lists available at ScienceDirect

Journal of Orthopaedic Translation

journal homepage: www.journals.elsevier.com/journal-of-orthopaedic-translation

Original Article

MiR-21 nanocapsules promote early bone repair of osteoporotic fractures by stimulating the osteogenic differentiation of bone marrow mesenchymal stem cells

Xiaolei Sun [a,b], Xueping Li [a], Hongzhao Qi [c], Xin Hou [a], Jin Zhao [a,**], Xubo Yuan [a,*], Xinlong Ma [b]

[a] Tianjin Key Laboratory of Composite and Functional Materials, School of Materials Science and Engineering, Tianjin University, Tianjin, 300072, China
[b] Department of Orthopaedics, Tianjin Hospital, Tianjin, 300211, China
[c] Institute for Translational Medicine, Qingdao University, Qingdao, 266021, China

ARTICLE INFO

Keywords:
Bone repair
MicroRNA-21
Nanocapsules
Osteoporotic fractures

ABSTRACT

Objective: The healing of osteoporotic fractures in the elderly patients is a difficult clinical problem. Currently, based on the internal fixation of fractures, the available drug treatments mainly focus on either inhibiting osteoclast function, such as bisphosphonate, calcitonin, oestrogen or promoting osteogenesis, such as parathyroid hormones. However, the availability of current antiosteoporotic drugs in promoting osteoporotic fracture healing is limited. The objective of the present study was to investigate the ability of the MiR-21/nanocapsule to enhance the early bone repair of osteoporotic fractures.

Methods: Based on the presence of matrix metalloproteinases that are overexpressed at the fracture site, we designed the matrix metalloproteinase–sensitive nanocapsules which were formed by in situ free radical polymerisation on the surface of MiR-21 with 2-(methacryloyloxy) ethyl phosphorylcholine and the bisacryloylated VPLGVRTK peptide. The MiR-21/nanocapsule [n (miR-21)] and O-carboxymethyl chitosan (CMCS) were mixed until they formed a gel-like material [CMCS/n (miR-21)] with good fluidity and injectability. Thirty elderly Sprague Dawley (SD) rats (female, 14-month-old, 380 ± 10 g) were subjected to bilateral removal of the ovaries (ovariectomised). All rats were subjected to bilateral bone defects (2 mm diameter) of the proximal tibia and randomly divided into three groups (groups A, B, and C): separately injected with CMCS/n (miR-21), CMCS/n (NC-miR), and saline. Micro-computed tomography (CT) imaging was performed to evaluate newly formed bone volume and connectivity. Nondecalcified histology and toluidine blue staining were performed to measure the effects of CMCS/n (miR-21) on bone repair. In vitro, the effect of n (miR-21) on osteogenic differentiation to bone marrow mesenchymal stem cells (BMSCs) which derived from the ovariectomised rat model was observed.

Results: The morphology of n (miR-21) was a regular spherical nanocapsule with a uniform small size (25–35 nm). The results confirmed that n (miR-21) could be efficiently phagocytosed by BMSCs and released in the cytoplasm to promote osteogenesis. The expression level of alkaline phosphatase and Runt-related transcription factor 2 mRNA in the n (miR-21) group was higher than that in the n (NC-miR) group. Animal experiments proved that CMCS/n (miR-21) produced better bone repair compared with the CMCS/n (NC-miR) group in the early stages of fracture healing at 4 weeks. In the late stage of fracture healing (8 weeks), micro-CT quantitative analysis showed that the new bone trabeculae in the CMCS/n (miR-21) group has decreased compared with the CMCS/n (NC-miR) group. In the CMCS/n (miR-21) group, the new cancellous bone had been absorbed, and the process of bone healing was almost completed. In contrast, the new bone in the CMCS/n (NC-miR) and the control groups was still in the healing process.

Conclusion: The cytological tests confirmed that n (miR-21) can promote osteogenic differentiation of BMSCs derived from the osteoporosis rat model. Furthermore, the results of animal tests demonstrated that local injection of CMCS/n (miR-21) promoted the early healing of osteoporotic bone defects. Consequently CMCS/n (miR-21) promoted the bone repair process to enter the moulding phase earlier.

* Corresponding author.
** Corresponding author.
E-mail addresses: zhaojin@tju.edu.cn (J. Zhao), xbyuan@tju.edu.cn (X. Yuan).

https://doi.org/10.1016/j.jot.2020.04.007
Received 8 January 2020; Received in revised form 10 April 2020; Accepted 16 April 2020
Available online 19 May 2020

The translational potential of this article: CMCS/n (miR-21) can be widely applied to elderly patients with osteoporotic fractures. This method can help patients with osteoporotic fractures recover earlier and avoid serious complications. It provides a potential approach for the clinical treatment of osteoporotic fractures in the elderly.

Introduction

With a growing aged population, the prevalence of osteoporotic fracture is projected to increase substantially. The process of bone remodelling is a physiological balance between osteoblasts forming new bone and osteoclasts absorbing the bone matrix [1]. The bone healing process is a complex physiological process that involves bone tissue regeneration and bone remodelling [2]. There are a variety of factors that affect fracture healing and remodelling. In elderly patients with osteoporosis, changes in hormone levels after the menopause and reduced cell proliferation make the bone healing process more difficult and slower after fracture. This can lead to complicated clinical problems, such as delayed fracture healing, fracture nonunion, and even postoperative fractures [3].

Growth factors play an important role in fracture healing. A haematoma microenvironment rapidly forms after fracture, and an inflammatory reaction occurs in the fracture site. During this process, a large number of growth factors (such as transforming growth factor-β (TGF-β), vascular endothelial growth factor (VEGF), and bone morphogenetic protein-2 (BMP-2)) locate to the fracture site [4]. These factors promote vascularisation and simultaneously recruit various types of stem cells from peripheral blood and induce their differentiation into osteoblasts to accelerate fracture repair [5]. At present, calcium, bone resorption inhibitors, and parathyroid hormones are widely used in the treatment of osteoporotic fracture [6]. These treatments can only improve the condition of osteoporosis and cannot directly promote bone healing. In addition, a variety of growth factors (BMP-2, plasma rich in growth factors (PRGF), platelet derived growth factor-BB (PDGF-BB) and SDF) have been applied to accelerate bone healing in osteoporotic fractures [7, 8]. MicroRNAs (miRNAs) are small, noncoding RNAs of 19–25 nucleotides that negatively regulate gene expression after transcription. MiRNAs degrade mRNA and inhibit translation by specifically binding to mRNA of the target gene in the 3-untranslated region (3′-UTR) [9]. The gene encoding the miR-21 primary transcript (pro-miR-21) is located in the intron region of TMEM49. The transcription of pro-miR-21 is initiated by the promoter of pro-miR-21 and terminated by the poly-A tail. Finally, pro-miR-21 was processed into mature miR-21 [10]. In the bone metabolism environment, miR-21 are mainly secreted from various cells such as osteoblasts, osteoclasts, bone marrow mesenchymal stem cells (BMSCs), and so on and regulate the cell-to-cell communication in the form of the exosome complex [11]. In addition, another part of miR-21 is located in the peripheral blood or tissue matrix. MiR-21 plays a considerable role in bone remodelling by regulating osteoblast and osteoclast differentiation. An increasing number of miRNAs have been shown to

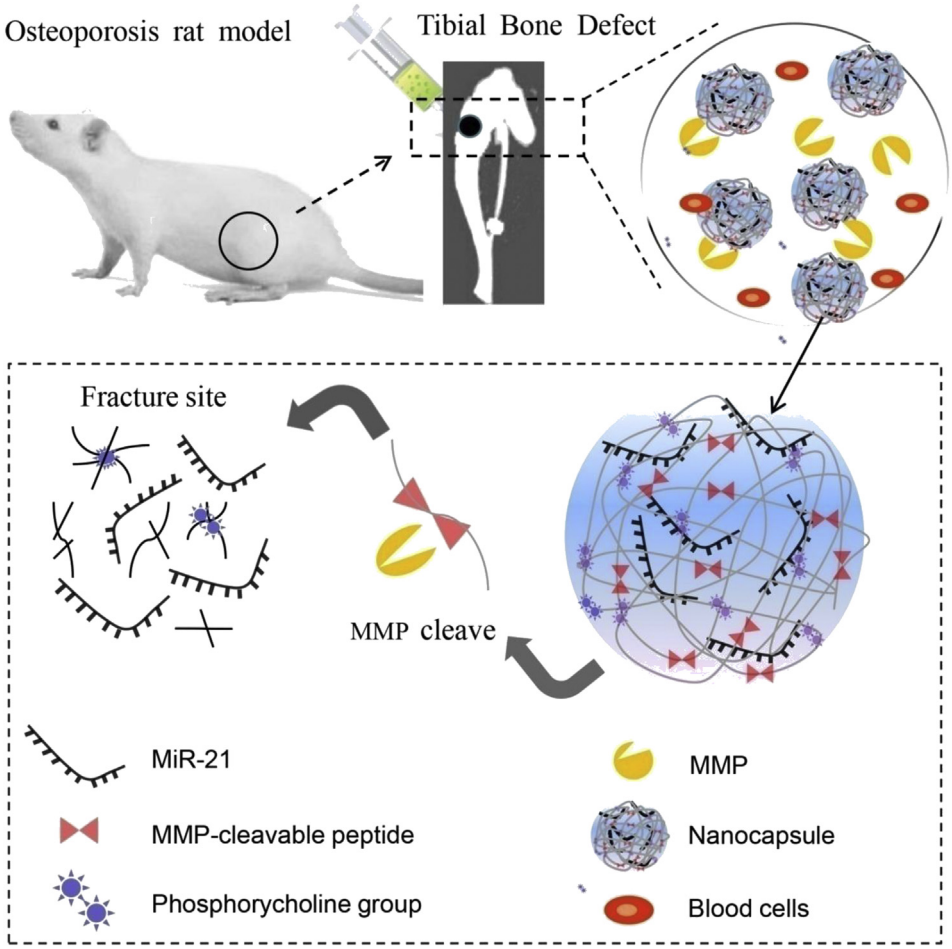

Scheme 1. A schematic illustrating the degradation and release of MMP-responsive n (miR-21) in the inflammatory environment (mainly contains MMP-2 and MMP-9) of the bone defect site. The proximal tibial bone defect model is achieved in osteoporotic rats (ovariectomised, OVX). MMP, matrix metalloproteinase.

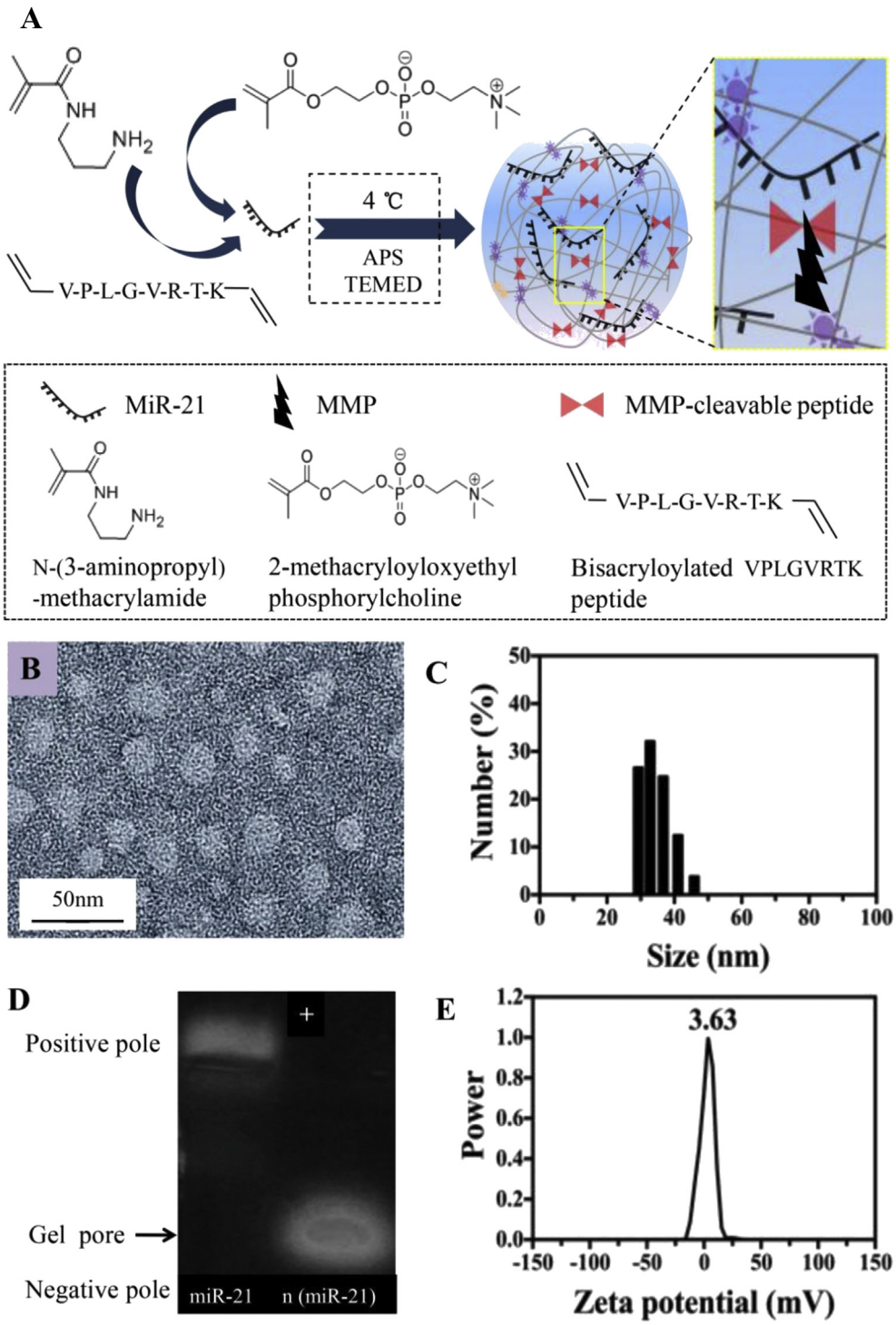

Figure 1. (A) A schematic illustrating the synthesis mechanism of MMP-responsive miR-21 nanocapsules n (miR-21) (B) A representative TEM image of n (miR-21) (scale bar, 50 nm) (C) Size distribution of the nanocapsules measured via DSL (D and E) Agarose gel electrophoresis and zeta potential of n (miR-21) (molar ratio = 4000:1). MMP, matrix metalloproteinase; TEM, transmission electron microscopy; DSL, dynamic light scattering.

participate in osteoblast formation, differentiation, apoptosis, and resorption in the repair of nonosteoporotic bone defects [12]. MiR-21 is expressed at a low level in the bone tissue and serum of patients with osteoporosis, and MiR-21 is a potential therapeutic target for osteoporosis [13].

The application of growth factors or miRNAs to a fracture site has the following caveats: digestion and removal (short half-life), poor targeting of the fracture site, large drug dosage but low drug utilisation, difficulty in localisation, inaccurate delivery, and infection [14,15]. A method that can protect growth factors or miRNAs from destruction by the body's enzymes and immune system and yet effectively deliver the factors or miRNAs to a fracture site is urgently needed. Therefore, an injectable carrier based on nanotechnology that can protect its cargo and achieve sustained release is a promising strategy. Targeted delivery of nerve growth factor (NGF) using nanocapsules has been achieved in the brains of Parkinson disease model mice [16]. However, no study has demonstrated whether local injection of miR-21 can promote the healing of osteoporotic fractures or the osteogenic differentiation of BMSCs from

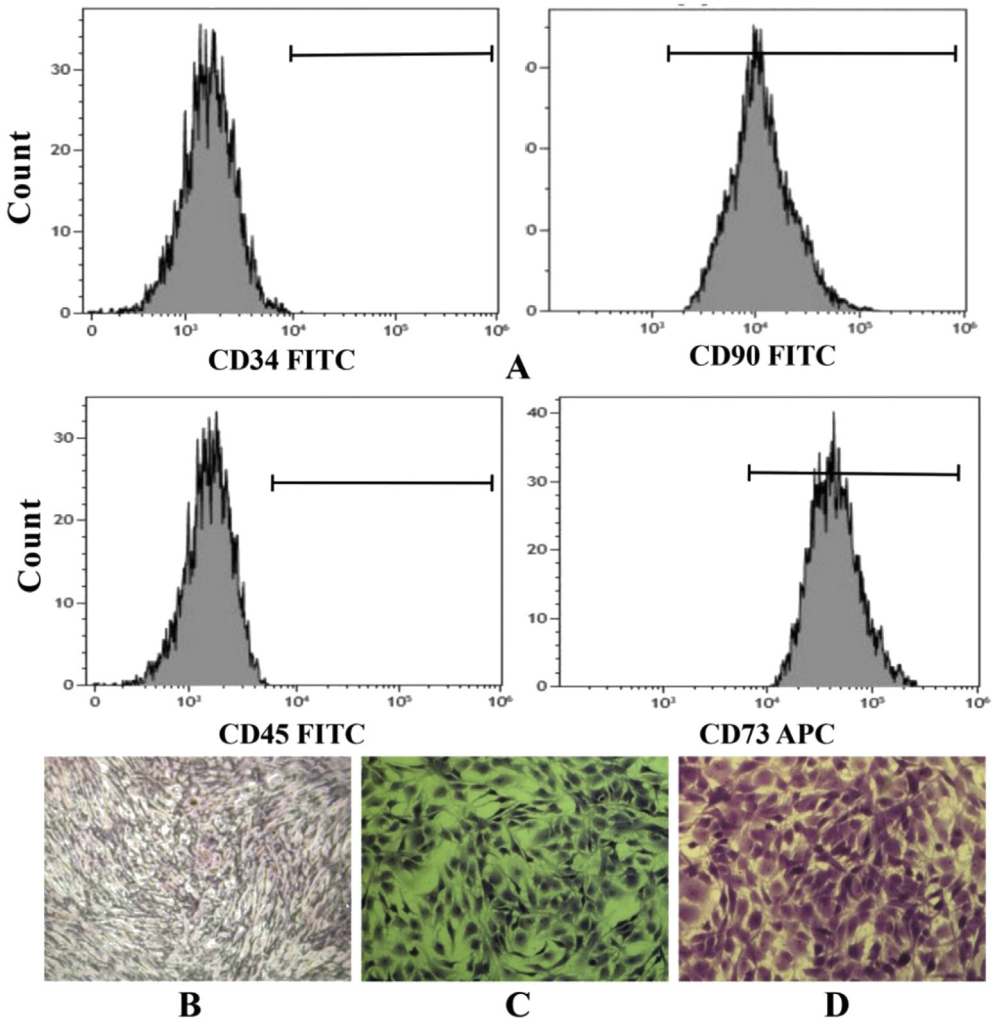

Figure 2. (A) The characterisation of the BMSCs by flow cytometry. The potential of triple lineage differentiation of BMSCs: (B) ALP staining (C) Toluidine blue staining (D) Oil red O staining. BMSCs, bone marrow mesenchymal stem cells. BMSCs, bone marrow mesenchymal stem cells.

osteoporotic rats. To address this challenge, we conceived an injectable nanocapsule-based carrier containing miR-21, which can continually release miR-21 at a fracture site.

As illustrated in Scheme 1, 2-methacryloyloxyethyl phosphorylcholine monomer and matrix metalloproteinase (MMP) cleavable peptide cross-linker form the Poly 2-methacryloyloxyethyl phosphorylcholine (PMPC) shell on the surface of miR-21 by in situ polymerisation. The PMPC shell can effectively stabilise miR-21. In the inflammatory microenvironment of the fracture site, the MMPs (mainly MMP-2 and MMP-9) were largely secreted to the fracture site to degrade proteins during the bone repair process [17]. The PMPC shells with unique enzyme responsiveness can be specifically degraded by MMPs. Based on the MMP enzyme responsiveness of the polymer shell, n (miR-21) can be sustained release at the fracture site. In this study, we explored the effect of n (miR-21) on the healing process of osteoporotic fractures and provided a new alternative method to accelerate the healing of osteoporotic fractures.

Material and methods

Materials and reagents

All chemical regents used were of analytical grade. Unless stated otherwise, all reagents were purchased from Sigma-Aldrich (St. Louis, MO, USA). The MiR-21 sequence was obtained from miRBase (http://microrna.sanger.ac.uk). The miRNAs were synthesised by GenePharma (Shanghai, China). miRNA sense strand sequences were: MiR-21: 5′-UAGCUUAUCAGACUGAUGUUGA-3′, and miRNA negative control (NC-miR): 5′-UUCUCCGAACGUGUCACGUTT-3′. TRIzol was supplied by Invitrogen (CA, USA). N-(3-aminopropyl)-methacrylamide was purchased from RuitaiBio (Beijing, China). ABC-peroxidase and diaminobenzidine were obtained from Boster Biotechnology (Wuhan, China). Antibodies were supplied by Santa Cruz Biotechnology (Santa Cruz, CA, USA).

Fabrication and characterisation of MiR-21 nanocapsules

The miR-21 (20 μM) or microRNA negative control (miR-NC) sample was dissolved using 10 μL RNase-free water in an ice-bath. N-(3-Aminopropyl) methacrylamide, acrylamide, and ethylene glycol dimethacrylate according to a molar ratio of 4:4:2 were dissolved in RNase-free water and mixed with microRNAs in a 200 μL centrifuge tube. Then, add 1 μL of 1% (w/v) ammonium persulfate and 2 μL of 1% (w/v) N,N,N′,N′-tetramethylethylenediamine into the microcentrifuge tube. The concentration of the final microRNAs in the RNase-free water was 5 μM in solution. The reaction was carried out at 4 °C for 2 h. Then the prepared microRNA nanocapsules were dialysed against a 10-KDa molecular weight dialysis bag in 4 °C phosphate buffer saline (PBS) to remove unreacted monomers and initiators. It was detected by agarose gel electrophoresis whether the nanocapsules were effectively entrapped for microRNAs. First, a 2% (w/v) agarose gel (containing 0.5 mg/mL ethidium bromide) was applied in 1 × TAE buffer and react for 20 min at

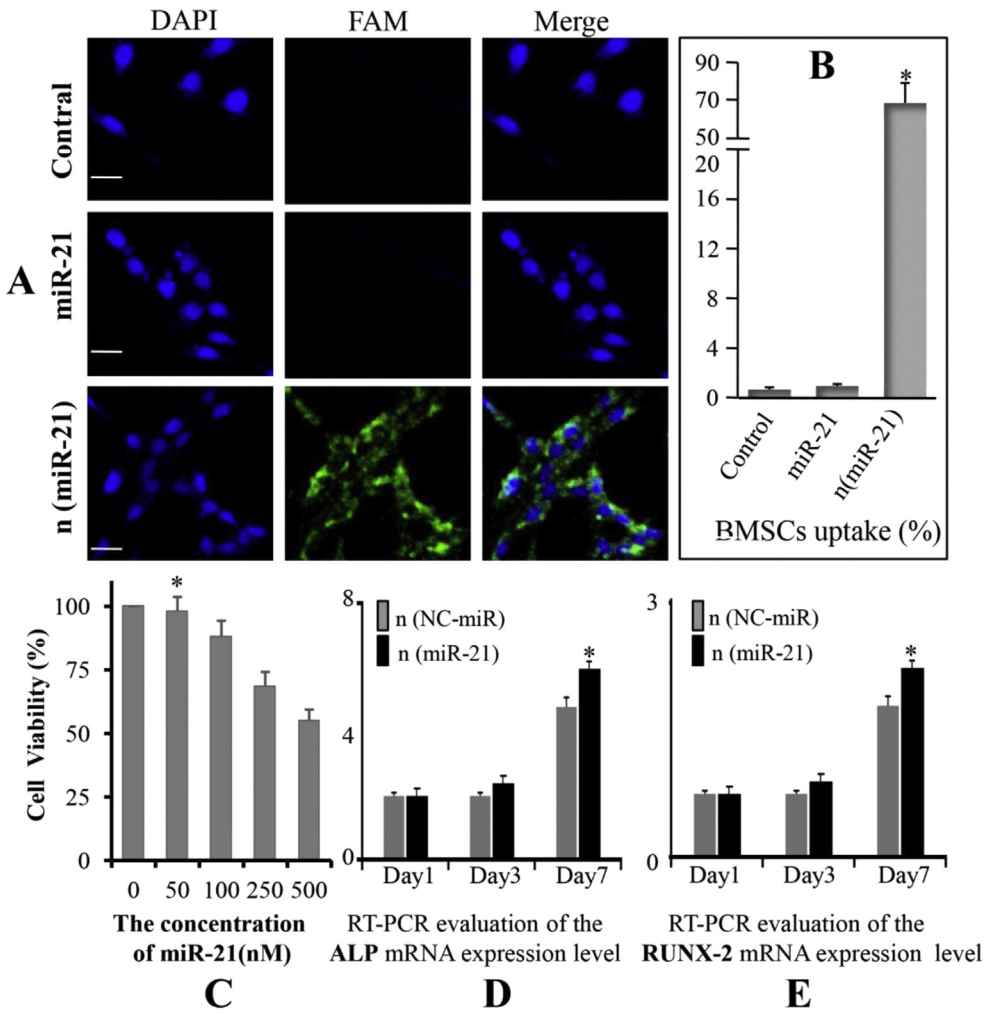

Figure 3. (A) Intracellular uptake analysis of the nanocapsules as assessed by confocal microscopy after 24h incubation with 50 nM FAM (carboxyfluorescein)-labelled (scale bar, 200 μm) (B) Quantitative analysis of cell uptake by flow cytometry. Each experiment was performed three times (*$p < 0.05$ vs. control and miR-21) (C) The cytotoxicity of the n (miR-21) in BMSCs with different concentrations of n (miR-21) (n = 5; *$p < 0.05$ vs. concentration of 100,250 and 500 nM) (D and E) The expression of early osteogenesis-related genes (ALP and RUNX-2) incubated with n (miR-21) and n (NC-miR) (*$p < 0.05$). BMSCs, bone marrow mesenchymal stem cells.

80 V. Finally, the image was collected by a 365 nm UV gel imaging system and observed the position of the microRNAs in the strip. The prepared MiR-21 nanocapsules [n (miR-21)] and negative control miRNA nanocapsules [n (NC-miR)] were stored at 4 °C for short-term storage. The size distribution and ζ-potential of n (miR-21) were measured via dynamic light scattering using a Zetasizer Nano instrument (Brookhaven, NY, USA), and samples were measured three times. The morphology was assessed by staining samples with 2% phosphotungstic acid and observation by transmission electron microscopy (TEM) (Jem-2100 f, JEOL, Japan). To prepare the TEM samples, 5 μl nanocapsules were drip on carbon-coated copper grids. After 5 min, the excess amount of samples was removed, and the grid was rinsed. FAM (carboxyfluorescein)-labelled MiR-21 (FAM-miR-21) was encapsulated in nanocapsules, which were then coated with O-carboxymethyl chitosan (CMCS) and observed by Ultra VIEW Vox confocal imaging (PerkinElmer, Fremont, CA, USA).

Preparation of CMCS/n(miR-21)

Nanocapsules were allowed to form at 4 °C for 2 h in a nitrogen atmosphere in 1.5 mL nonstick, sterile, RNase-free microfuge tubes. CMCS powder (200 μg) and 100 μL of the miRNA nanocapsules (containing 2 nmol MiR-21 or 2 nmol NC-miR) were mixed until they were completely dissolved into a semisolid gel material. CMCS/n (miR-21) and CMCS/n (NC-miR) were used for animal experiments. After sample preparation, CMCS/n (miR-21) was incubated on ice for 30 min and stored at 4 °C until use.

Intracellular uptake of n (miR-21) and the expression of alkaline phosphatase and Runt-related transcription factor 2 genes

BMSCs were isolated from osteoporotic ovariectomised (OVX) rats (n = 3). The isolation, ex vivo expansion, and characterisation of BMSCs were performed as previously described before incubation with n (miR-21). The specific surface markers CD 73, CD 90, CD 34, and CD 45 of BMSCs were analysed by flow cytometry. Alkaline phosphatase (ALP) staining, toluidine blue staining, and oil red O staining, respectively, was used to detect the potential of triple lineage differentiation of BMSCs. The basic culture medium for isolating BMSCs was complete DMEM/F-12 (DF-12, Hyclone, Logan, UT, USA) containing 10% foetal bovine serum (Gibco, USA), 100 U/mL penicillin, and 100 mg/mL streptomycin. The BMSCs at passage three were cultured in 96-well plate for 2 days after treatment with different concentrations of n (miR-21) (0, 50, 100, 250 and 500 nM). The cytotoxicity of the n (miR-21) was detected by MTT (3-(4,5-dimethyl-2-thiazolyl)-2,5-diphenyl-2-H-tetrazolium bromide) assay. To evaluate the phagocytosis of n (miR-21), BMSCs isolated from the osteoporotic rat model with a density of 1×10^4 cells per well were seeded on twelve-chamber slides and cultured for 48 h at 37 °C. Then BMSCs were treated for 4h with culture media in the presence of n (miR-21) labelled with FAM. After 4h incubation, the cells were washed twice with PBS and fixed with methanol for 15 min. After PBS washing twice, cells were labelled with DAPI (4',6-diamidino-2-phenylindole) for 3 min. After PBS washing, the cells were stored at 4 °C and protected from light. The efficiency of intracellular uptake of each group was assessed by flow cytometry and confocal microscopy, and untreated cells were used as the

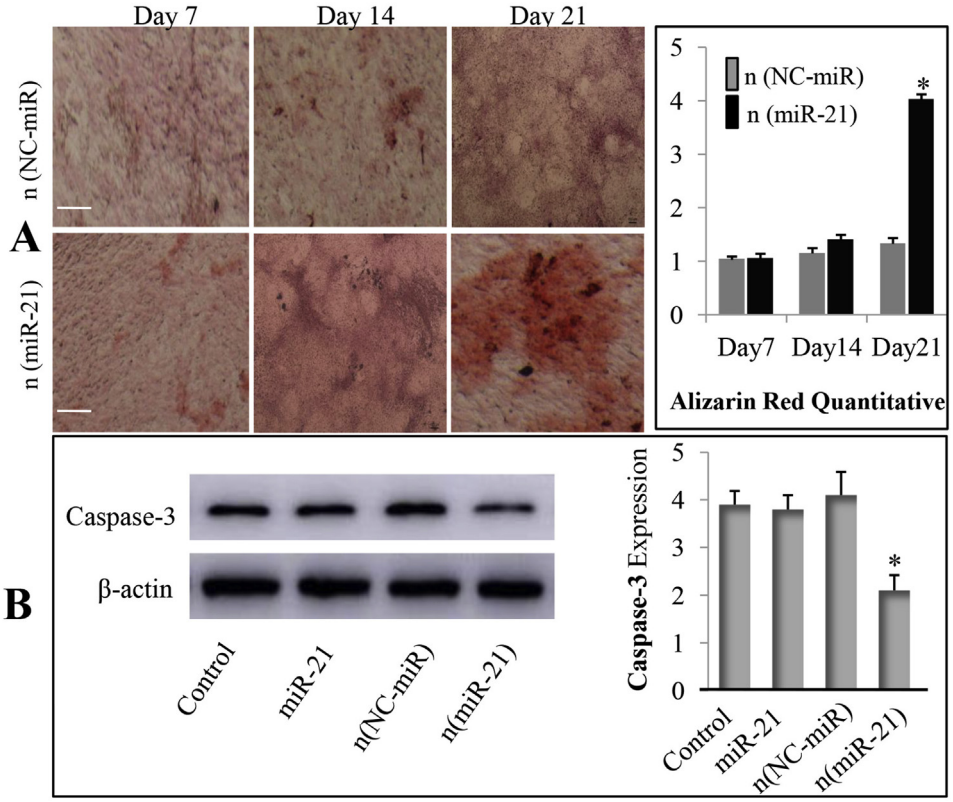

Figure 4. (A) Alizarin red staining analysis was performed at days 7, 14, and 21 after treatment of the MiR-21 to visualise calcium nodule accumulation in BMSCs (40x); Quantitative analysis of alizarin red staining was performed using ImageJ (*$p < 0.05$) (B) Western blot analysis of apoptosis-related caspase-3 protein expression on day 5 after miR-21 nanocapsules treated BMSCs. Quantitative analysis of the immunoblots was determined by ImageJ (*$p < 0.05$). BMSCs, bone marrow mesenchymal stem cells.

control. In addition, we observed the expression of ALP and Runt-related transcription factor 2 (RUNX-2) genes by quantitative real-time polymerase chain reaction (PCR) at days 1, 3, and 7 after MiR-21 treatment. Total RNA was extracted from cultured cells with TRIzol reagent (Qiagen, Valencia, CA, USA), according to a standard protocol. A nanodrop spectrophotometer (Gene) was used to determine the concentration of total mRNA. Real-time PCR (Bio-Rad, USA) was used for PCR amplification. The following primers were used: ALP, forward 5′-GGACCATTCCCAC GTCTTCAC-3′ and reverse 5′-CCTTGTAGCCAGGC CCATTG-3′; RUNX-2, forward 5′-CCCGTGGCCTTCAAGGT-3′ and reverse 5′-CGTT ACCCGCCATGACAGTA-3′. The mouse β-actin gene was used as the internal control. Reaction conditions were 40 cycles at 95 °C for 3 min, 95 °C for 15 s, and 60 °C for 30 s. All the expression data were calculated from the cycle threshold value using the cycle threshold method. All real time-polymerase chain reaction (RT-PCR) reactions were performed in triplicate. The mineralisation of the BMSCs was detected by alizarin red staining at days 7, 14, and 21 after treatment with microRNA nanocapsules. Using Western blot analysis, the expression level of apoptosis-related protein caspase-3 was analysed on day 5 after microRNA nanocapsules treated BMSCs. The density of the immunoblots was determined by ImageJ analysis software.

Animal experiment

To study the ability of the n (miR-21) to enhance the early bone repair of osteoporotic fractures, an osteoporotic bone defect model was generated in Sprague Dawley (SD) rats. Elderly 14-month-old female SD rats (body weight, 380 ± 10 g) were provided by the experimental animal center of Tianjin Hospital. The experimental protocol was approved by the Institutional Animal Care and Use Committee of Tianjin Medical University. As an osteoporotic model, 30 rats were subjected to bilateral removal of the ovaries. Ten rats in the sham group were incision and sutured without removal of the ovaries (SHAM). At 3 months after the procedure, the lumbar bone mineral density was measured by dual energy X-ray absorptiometry (DEXA) (Hologic Discovery, USA) and the trabecular bone microarchitecture of the lumbar was measured using a microtomography CT (Inveon Siemens, Germany). We observed the efficiency of the release of n (miR-21) in the bone defect after the 24 h injection of miR-21 labelled FITC (fluoresceine isothiocyanate). The OVX rat with tibial bone defect was used to evaluate the release efficiency of n (miR-21) on the fractured part. The normal group and the sham operation group with only skin cut were used as the control group. All rats were subjected to bilateral bone defects (2 mm diameter) of the proximal tibia and randomly divided into three groups (groups A, B, and C): In Group A (n = 10) the defect was injected with CMCS/n (miR-21), in Group B (n = 10) the defect was injected with CMCS/n (NC-miR), and in Group C (n = 10) the defect was injected with saline. Under anaesthesia (6% sodium pentobarbital, 60 mg/kg), a 1-cm incision was made to the proximal area of the tibia to expose the tibia, and a 2-mm diameter round defect was created in cortical the and cancellous bone using a dental drill (SU 100, BEGO, Germany) under constant irrigation with 0.9% saline. The defects were injected with CMCS/n (miR-21), CMCS/n (NC-miR), or saline (control group). In animal experiments, the semisolid gel was injected into bone defects (2 mm in diameter) using an injector with a needle of 1.5 mm diameter. Using an injector with a wider needle, the semisolid gel can be smoothly injected into the bone defects and effectively coagulated at the bone defect site. The procedure was performed in a sterile environment, and the animals were placed on a heating pad to maintain their body temperature during the operation. After surgery, all rats were individually caged and fed. Rats were sacrificed at 4 or 8 weeks after surgery, and the tibias were dissected. BMSCs were respectively isolated from osteoporotic OVX rats at 4 weeks after n (miR-21) and n (NC-miR) treatment. Cells at passage three were incubated in six-well plates with a density of 1×10^4 cells per well. Quantitative analysis of ALP expression and calcium deposition in each experimental group was used to evaluate the osteogenic differentiation potential of BMSCs isolated from OVX rats at 4 weeks. Five right tibias from each group were fixed with 75% ethanol and collected for nondecalcification sections and

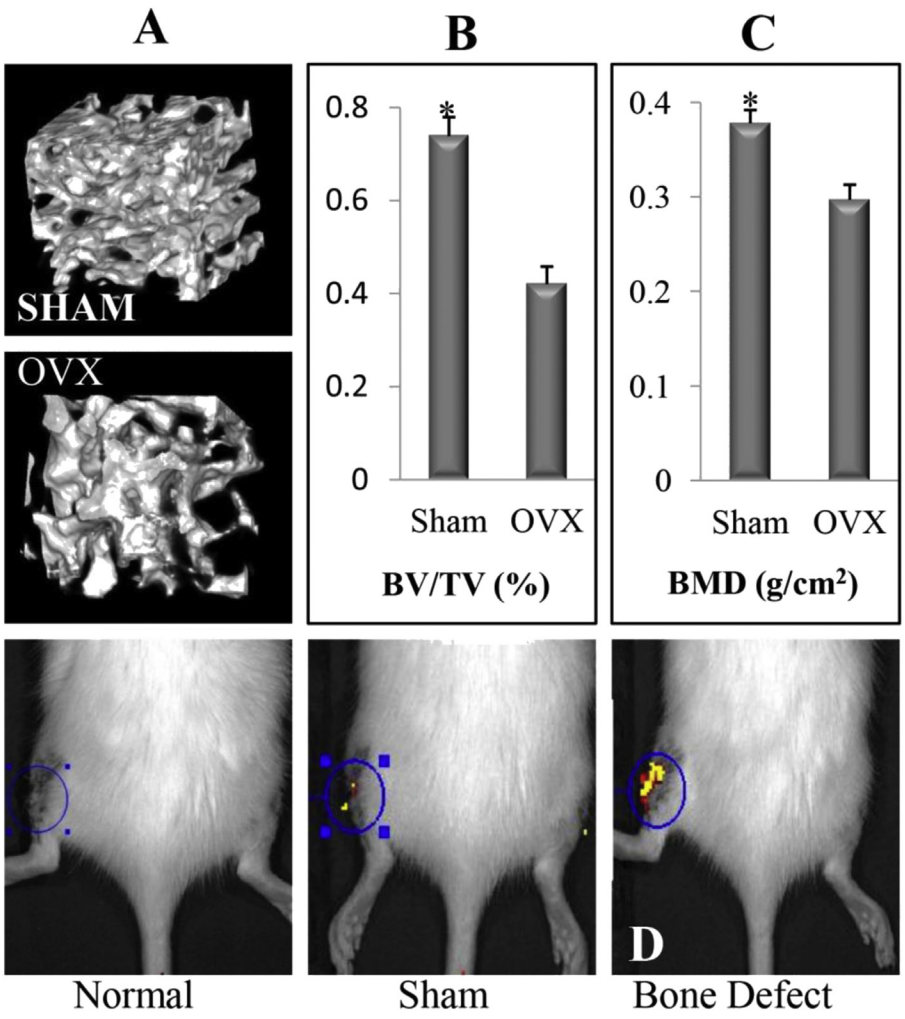

Figure 5. (A) 3D images of representative lumbar cancellous bone in the SHAM and OVX group (B) Result of lumbar BMD by DEXA in the sham and OVX group (C) Micro-CT quantitative analysis of lumbar cancellous bone (BV/TV, %) (n = 10; *$p < 0.05$ vs. OVX group) (D) Fluorescence intensity of the bone defect after the 24 h injection of miR-21 labelled FITC. BMD, bone mineral density; OVX, ovariectomised; DEXA, dual energy X-ray absorptiometry; FITC, fluoresceine isothiocyanate.

toluidine blue staining. Three discontinuous histological sections were taken from each sample, and five fields of view were randomly selected from each section. ImageJ software was used to quantitatively analyse the trabecular bone volume ratio (BV/TV, %) and the cortical bone thickness (mm) to evaluate the newly formed bone. A light microscope (TE2000U, Nikon, Japan) was used to view the nondecalcification sections and HE stain. The remaining samples from each experimental group were fixed in 4% paraformaldehyde solution and scanned at a slice thickness of 21 μm and the voxel resolution of 22 μm^3 using a micro-computed tomography (CT) system (Inveon Siemens, Germany). 3D images were redigitised at a 16-bit data format and obtained for visualisation. The newly formed cancellous bone with a diameter of 2 mm at the bone defect site was defined as the region of interest. Bone morphometric parameters including bone volume/total volume (BV/TV; %), trabecular thickness (Tb.Th; μm), and trabecular number (Tb.N; 1/mm) were measured by analysing the volume of interest (VOI) using analysis software provided by the instrument.

Statistical analysis

The data are presented as the mean ± standard deviation (SD). Data were compared by two-tailed t test or one-way ANOVA for experiments with more than two subgroups. Differences with a value of $p < 0.05$ were considered significant. All statistical evaluations were performed with SPSS17.0 (SPSS, Chicago, USA).

Results

Preparation and characterisation of n(miR-21)

MiR-21 was encapsulated in nanocapsules which were prepared as described in Fig. 1A.

Using N-(3-Aminopropyl) methacrylamide and 2-methacryloyloxyethyl phosphorylcholine as monomers and the bisacrylated MMP-2-responsive peptide as a cross-linker, the n (miR-21) was synthesised by in situ polymerisation. Under electrostatic interaction and hydrogen bonding interaction, the monomer and cross-linker formed a degradable polymer shell around the surface of the miR-21 at 4 C. Ammonium persulfate and N,N,N′,N′-tetramethylethylenediamine triggered the polymerisation between monomers and the cross-linker. The TEM image shows that the morphology of n (miR-21) was a regular spherical nanocapsule with a uniform diameter of 25–35 nm (molar ratio = 4000:1) (Fig. 1B). The dynamic light scattering (~32.6 nm) measurement was consistent with the TEM observation (Fig. 1C). Fig. 1 D shows a gel electrophoresis assay of the nanocapsules (prepared with the M:R ratios 4000:1). The gel electrophoresis showed that native miR-21 shifted to the positive electrode. For comparison, the n (miR-21) are trapped in the loading wells without significant electrophoresis shift. The result indicated that miR-21 was covered by a neutral polymer shell. Furthermore, the mean zeta potential of n (miR-21) was nearly 0 mV because of the shielding effect of the neutral polymer shell (Fig. 1E). The results of gel

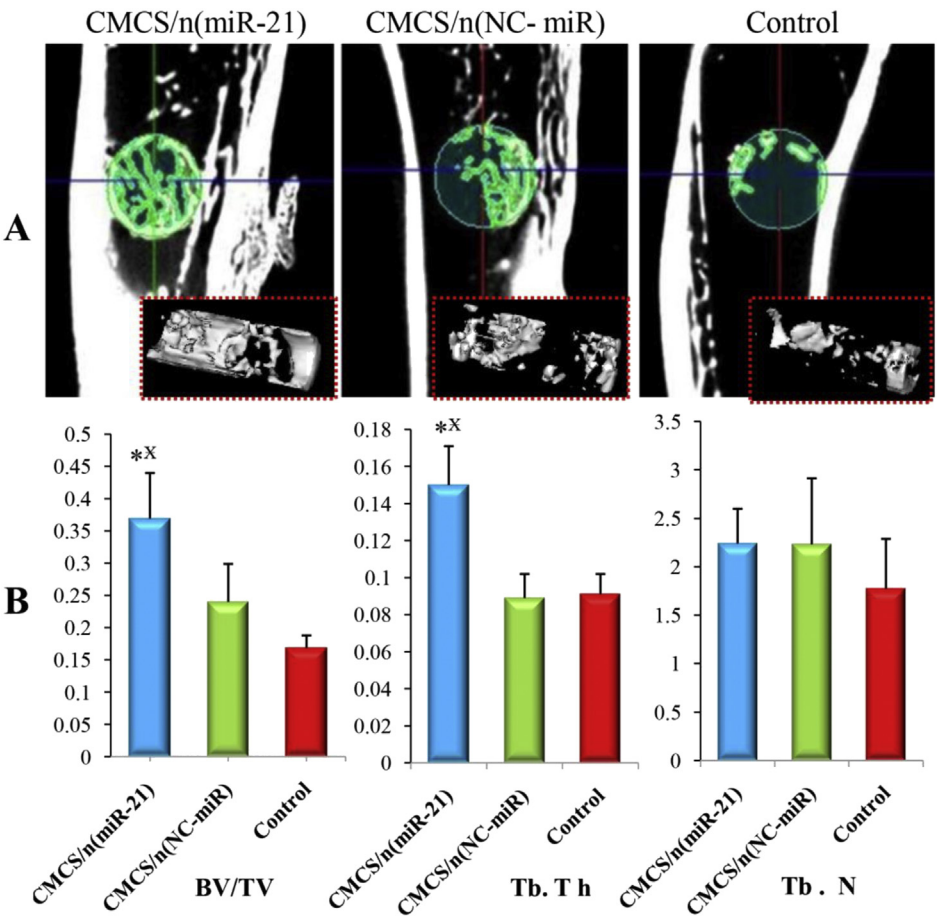

Figure 6. (A) Micro CT images of representative rat tibias at 4th week: 3D architecture of trabecular within the distal tibias (B) Quantitative analysis of the new trabecular bone volume (BV/TV), trabecular thickness (Tb.Th), and trabecular number (Tb.N) of the bone defect in OVX rats by microtomography analysis (n = 5; $^{*}p < 0.05$ vs. CMCS/n (miR-NC) group; $p < 0.05$ vs. control group.). OVX, ovariectomised.

electrophoresis and zeta potential both confirmed that the encapsulate efficacy of the nanocapsules for MiR-21 was satisfactory. The aforementioned results indicate that the nanocapsules have a uniform spherical structure with appropriate size and zeta potential. Nanocapsules are potential excellent carriers for delivery of miR-21.

Effect of n (miR-21) on the osteogenic differentiation of BMSCs isolated from OVX rats in vitro.

Analysis of the cell-specific surface markers by flow cytometry showed that the cell population expressed CD 73 and CD 90, while lacked the expression of CD 34 and CD 45 (Fig. 2A). The results of ALP staining, toluidine blue staining, and oil red O staining confirmed that BMSCs derived from the OVX rat model can differentiate to osteoblasts (Fig. 2B), chondrocytes (Fig. 2C), and adipocytes (Fig. 2D) under standard differentiating conditions.

The result of confocal microscopy showed that significant green fluorescence was present in the cytoplasm of BMSCs after 4 h of incubation with n (miR-21) labelled with FAM (Fig. 3A). Little native miR-21 was taken up by BMSCs, similar to the control group. The efficiency of cellular uptake of microRNA by BMSCs was further quantitatively evaluated by flow cytometry. The results show that n (miR-21) can be taken up by BMSCs with a high efficiency (70.04%; Fig. 3B). Contrarily, no significant cellular uptake of native miR-21 was observed in the miR-21 group, similar to the control group. The n (miR-21) can effectively enter the cytoplasm of BMSCs, so that miR-21 can play a key role in inducing osteogenic differentiation of BMSCs. MTT results showed that the cytotoxicity of n (miR-21) increased significantly when the concentration was higher than 100 Nm (Fig. 3C). At a concentration of 50 nM, the BMSCs maintained a metabolic activity of 98.06% which indicated that n (miR-21) has better biocompatibility and lower cytotoxicity at this concentration. To investigate the effect of miR-21 on osteogenic differentiation of BMSCs obtained from OVX rats, the expression of ALP and RUNX-2 genes was determined on days 1, 3, and 7 after MiR-21 treatment. The levels of ALP mRNA in both groups were increased on day 3 and levels peaked at day 7. Furthermore, ALP mRNA levels in the MiR-21 group were higher than that in the NC-miR group ($^{*}p < 0.05$) (Fig. 3D). Similarly, the levels of RUNX-2 mRNA had the same trend and peaked at day 7 (Fig. 3E). Each value represents the mean ± SD from triplicate determinations.

The result of Alizarin red staining confirmed that BMSCs treated with the n (miR-21) showed more mineralisation compared with the n (NC-miR) group at days 21. Quantitative analysis using imageJ software showed that the BMSCs treated with n (mir-21) produced more calcium accumulation than those of the n (NC-miR) group (Fig. 4A). The Western blot bands and normalised intensity using imageJ software demonstrate that BMSCs treated with n (mir-21) produced the lowest levels of caspase-3 expression (Fig. 4B). Therefore, the expression of caspase-3 is inhibited, leading to the inhibition of BMSC apoptosis. These results prove that nanocapsules could be efficiently taken up by BMSCs and have better biocompatibility and lower cytotoxicity. Furthermore, Mir-21 promoted the expression of ALP and RUNX-2 genes in BMSCs isolated from OVX rats and inhibited the expression of caspase-3, thereby promoting the bone healing of osteoporotic bone defects.

The bone repair efficiency of CMCS/n (miR-21) in osteoporotic bone defect in vivo.

Quantitative analysis results indicated that both bone mineral density and cancellous bone mass were lower in the OVX group than that in

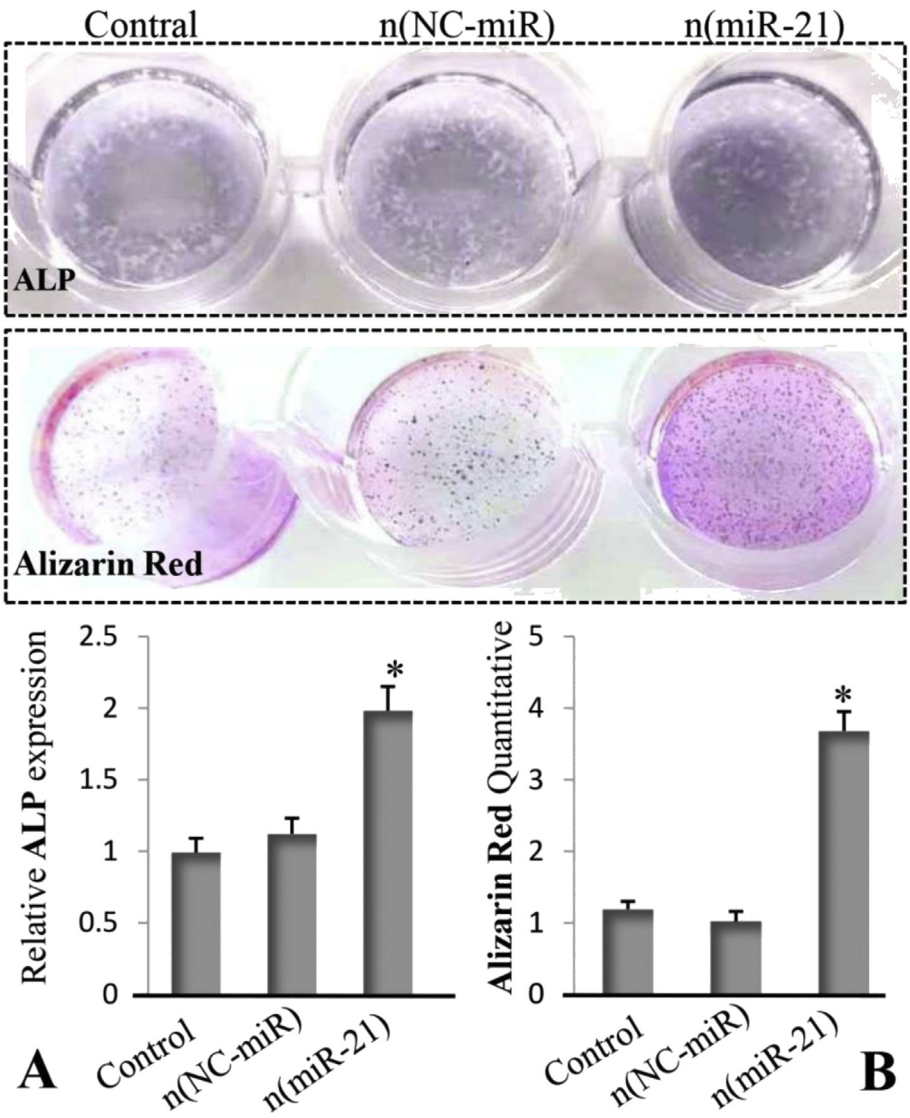

Figure 7. (A) Quantitative analysis of ALP expression of BMSCs isolated from OVX rats at 4 weeks. (B) Calcium deposition of BMSCs isolated from OVX rats at 4 weeks (n = 5; *$p < 0.05$ vs. n (NC-miR) and control group). OVX, ovariectomised; BMSCs, bone marrow mesenchymal stem cells; ALP, alkaline phosphatase.

SHAM group (Fig. 5B and C). The results showed that the OVX rat model was established successfully. After the 24 h of FITC-labelled miR-21 injection, a large amount of MMP at the bone defect site cleaved the nanocapsules and released the miR-21 labelled FITC. Therefore, high fluorescence intensity can be detected in the bone defect group (Fig. 5D). In sham operation group, because there was a small amount of MMP in the skin wound, low fluorescence intensity can be detected. There was no MMP in the normal group, so the fluorescence intensity cannot be detected.

To study the effect of CMCS/n (miR-21) in the bone healing process, a tibial bone defect of 2 mm in diameter was generated in aged OVX rats. Micro-CT imaging was performed to evaluate newly formed bone volume and connectivity. At 4 weeks, in the CMCS/n (miR-21) group, the defect site was significantly bridged with the new cancellous bone. In contrast, in the CMCS/n (NC-miR) and control groups, the defect site had less newly formed bone (Fig. 6A). Furthermore, micro-CT quantitative analysis showed that the BV/TV and Tb.Th in the CMCS/n (miR-21) group were significantly increased compared with those in the CMCS/n (NC-miR) and control groups ($p < 0.05$) (Fig. 6B). In addition, Tb.Th was not significantly different between the CMCS/n (miR-21) group and the CMCS/n (NC-miR) group.

The result of ALP quantitative analysis confirmed that BMSCs isolated from OVX rats treated with the n (miR-21) for 4 weeks showed more ALP expression compared with the n (NC-miR) and control groups (Fig. 7A). Similarly, quantitative analysis of alizarin red staining shows that the n (miR-21)-treated group had higher calcium nodule formation than that of the n (NC-miR) and control group (Fig. 7B).

At 8 weeks, micro-CT showed less new cancellous bone in the CMCS/n (miR-21) group than in the CMCS/n (NC-miR) and control groups (Fig. 8A). Meanwhile, quantitative micro-CT showed that the BV/TV in the CMCS/n (miR-21) group was significantly decreased compared with that in the CMCS/n (NC-miR) group. Similarly, Tb.Th in the CMCS/n (miR-21) group was significantly decreased compared with the control group ($p < 0.05$) (Fig. 8B).

In addition, nondecalcified histology and toluidine blue staining were performed to measure the effects of MiR-21 on bone repair. At 4 weeks, the analysis of imageJ confirmed that the new cancellous bone around the defect site was greatest in the CMCS/n (miR-21) group (Fig. 9A). In contrast, at 8 weeks, the new cancellous bone in the CMCS/n (miR-21) group had been absorbed and the marrow cavity had been dredged. In the CMCS/n (NC-miR) group, the cancellous bone in the defect area was still in the process of repair. Three different widths were taken at the

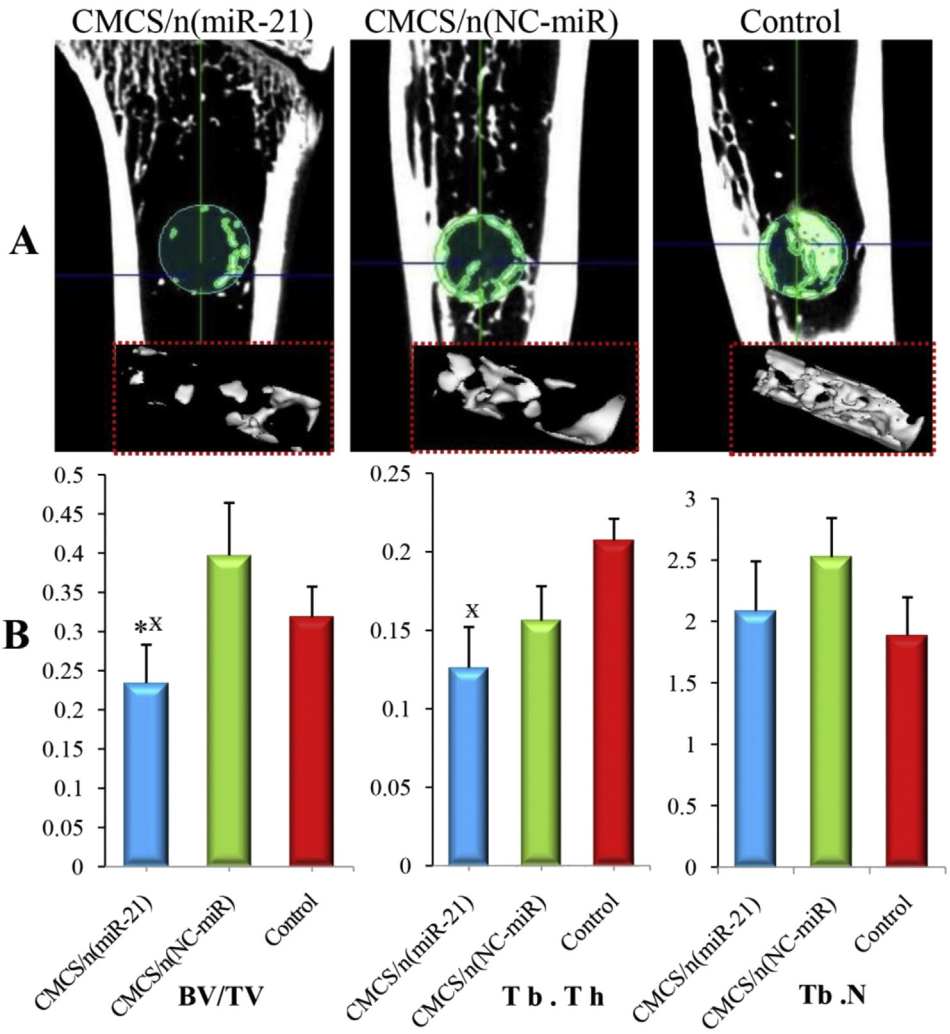

Figure 8. (A) Micro CT images of representative rat tibias at 4th week: 3D architecture of trabecular within the distal tibias (B) Quantitative analysis of the new trabecular bone volume (BV/TV), trabecular thickness (Tb.Th), and trabecular number (Tb.N) of the bone defect in OVX rats by microtomography analysis (n = 5; $^{*}p < 0.05$ vs. CMCS/n (NC-miR) group; $p < 0.05$ vs. control group.). OVX, ovariectomised.

bone defect site to quantitatively evaluate the average thickness of the newly generated cortical bone. In the CMCS/n (miR-21) group, the thickness of the newly formed cortical bone was thicker than that in the CMCS/n (NC-miR) group and the control group (Fig. 9B). Furthermore, the structure of the neocortical bone is similar to that of the original cortical bone. The results confirmed that local injection of MMP-sensitive CMCS/n (miR-21) can efficiently release miR-21 to bone defect sites. n (miR-21) could promote the early bone repair in osteoporotic bone defect by stimulating the osteogenic differentiation of BMSCs.

Discussion

Bone homoeostasis mainly depends on bone resorption by osteoclasts and bone formation by osteoblasts. ALP and RUNX-2 are markers of early osteogenic differentiation of BMSCs. Therefore, we examined the effects of MiR-21 on the osteogenic differentiation of mesenchymal stem cells by detecting the expression levels of early osteogenic markers (ALP and RUNX-2) and by measuring the formation of calcium nodules by alizarin red staining. MiR-21 has the potential to promote osteogenesis. ALP and RUNX-2 mRNA levels in the CMCS/n (miR-21) group were higher than those in the CMCS/n (NC-miR) or control groups. These results confirmed that MiR-21 is involved in promoting osteogenic differentiation of BMSCs by regulating expression of ALP and RUNX-2. Another interesting result was that the expression of both ALP and RUNX-2 gene was also increased in the n (NC-miR) group on day 7 after treatment. The nanocapsules used in the n (miR-21) and n (NC-miR) groups have the same structure, so the components of nanocapsule were not the main reason for the increased expression of ALP and RUNX-2 genes. The cultured BMSCs in vitro have lost self-renewal ability and experienced osteogenic differentiation on day 7 after treatment under DMEM medium, which ultimately resulted in the increased expression of ALP and RUNX-2 genes. Owing to the role of MiR-21 in promoting osteogenic differentiation, the expression of ALP and RUNX-2 gene in the n (MiR-21) group is still higher than that in the n (NC-MiR) group. In summary, MiR-21 accelerates bone healing of osteoporotic bone defects by promoting the early expression of ALP and RUNX-2 genes in BMSCs. The activation of caspase-3 is one of the most important events in the process of apoptosis. Our study confirmed that n (mir-21) inhibited the expression of caspase-3 in BMSCs isolated from OVX rats, leading to the inhibition of BMSC apoptosis. Previous research confirmed that overexpression of miR-21 could promote the survival of mesenchymal stem cells (MSCs) exposed to hypoxia [18]. In contrast, down regulation of miR-21 aggravated apoptosis of MSCs.

In this study, we used elderly ovariectomised rats with an initial age of 14 months as postmenopausal models, as these models are more representative of oestrogen deficiency and bone metabolism in the elderly. Moreover, the characteristics of bone loss are similar to elderly women with postmenopausal osteoporosis. Osteoporotic fractures occur

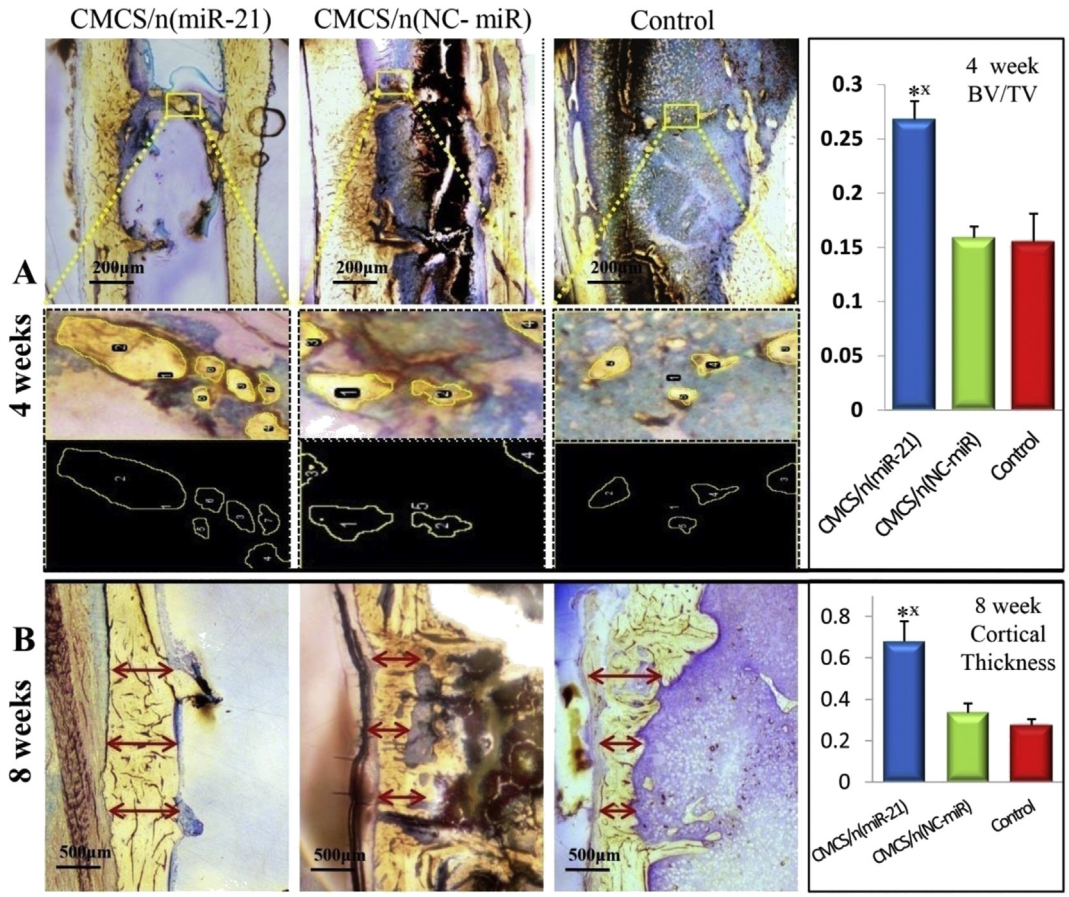

Figure 9. Nondemineralised hard tissue histology and toluidine blue stained for 4th and 8th weeks (A) At 4 weeks, the new cancellous bone (shown in the yellow frame) in the bone defect site was quantitatively analysed (BV/TV) by ImageJ (B) At 8 weeks, the thickness of the new formed cortical bone (red arrow) in the bone defect site was quantitatively analysed by ImageJ (n = 5; *$p < 0.05$ vs. CMCS/n (NC-miR) group; $p < 0.05$ vs. control group.

mostly in elderly patients suffering from a variety of diseases. In addition, patients with osteoporosis have impaired ability to repair fractured bone. Therefore, the healing of osteoporotic fractures takes longer than normal fractures [19,20]. Irrespective of whether patients receive surgery or conservative treatment, longer healing times for osteoporotic fractures increase the incidence of various serious complications, such as lower extremity venous thrombosis, pulmonary embolism, hypostatic pneumonia, and urinary tract infection [21,22]. Therefore, there is an urgent need to speed up the repair process of osteoporotic fractures to enable patients to resume functional exercise as soon as possible to reduce morbidity and mortality. Numerous studies have confirmed that miRNAs play important roles in the development of embryonic bone and repair after fracture [9,23]. Tokar et al. [24] reported that MiR-21 is expressed in cardiovascular diseases, cancer, and digestive system diseases and participates in their pathophysiological processes. Huang et al. [25] reported that MiR-320a inhibits BMSC differentiation into osteoblasts, and it was recently reported that MiR-21 promotes osteogenic differentiation of human umbilical cord stem cells [26]. However, the existing literature mostly focuses on the effects of miRNAs on the healing process of normal bone in young people. Few studies have focused on bone healing of osteoporotic fractures. Therefore, we investigated whether MiR-21 can promote the repair process of osteoporotic fractures by examining its effects on osteogenic differentiation of BMSCs derived from an osteoporotic animal model. Previous studies have shown that circulating mir-21 can reflect the risk of osteoporotic vertebral fractures in postmenopausal women. The downregulation of mir-21 was verified in the plasma of patients with osteoporosis and osteopenia [27]. MiR-21 has broad potential in the diagnosis and treatment of osteoporotic fracture.

During the early healing process of osteoporotic bone defects, quantitative micro-CT analysis showed more new cancellous bone in the CMCS/n (miR-21) group than that in the CMCS/n (NC-miR) and control groups. In the latter part of the repair process of osteoporotic bone defects, the new cancellous bone in the CMCS/n (miR-21) group had been absorbed and remodelled and the marrow cavity had been dredged, while in the CMCS/n (NC-miR) and the control groups, the cancellous bone was still in the process of repair and remolding. Toluidine blue staining of nondecalcified hard sections showed that bone healing in the CMCS/n (miR-21) group was fastest at 4 weeks. New cancellous was formed around the defect site in the CMCS/n (miR-21) group, and the cortical bone thickness was almost the same as that of the original cortical bone. After 8 weeks, in the CMCS/n (NC-miR) group, the defect area was still in the process of repair with more new cancellous bone. In contrast, the new cancellous bone in the CMCS/n (miR-21) group had been absorbed and remodelled. Furthermore, the marrow cavity in the defect area had been dredged. Patients with osteoporotic fractures should be rehabilitated as early as possible to avoid serious complications [28]. A previous study confirms that the key to the healing of osteoporotic fractures is early initiation of the bone repair phase [29–31]. In conclusion, both micro-CT and histological analyses showed that n (miR-21) promotes the early healing process of osteoporotic bone defects and consequently accelerates bone healing earlier into the moulding phase.

Conclusion

Local injection of MMP-sensitive CMCS/n (miR-21) can efficiently release miR-21 to bone defect sites. The structure and function of miR-21

were well maintained during the local injection. The results confirmed that n (miR-21) could promote the early bone repair in osteoporotic bone defect by stimulating the osteogenic differentiation of BMSCs. Local injection of CMCS/n (miR-21) can be widely applied to elderly patients with osteoporotic fractures who are not suitable for internal fixation surgery. Furthermore, the MMP-sensitive nanocapsules can be used to deliver other micro-RNA with osteogenic activity to accelerate the healing of osteoporotic fractures.

Conflict of Interest

The authors have no conflicts of interest to declare.

Acknowledgements

This work was supported by grants from the National Natural Science Foundation of China of China (No. 31600769; 81871777; 51673144), the Key Foundation of Tianjin Health Commission (No. 2017008).

References

[1] Sims NA, Walsh NC. Intercellular cross-talk among bone cells: new factors and pathways. Curr Osteoporos Rep 2012;10:109–17.
[2] Matsuo K, Irie N. Osteoclast-osteoblast communication. Arch Biochem Biophys 2012;473:201–9.
[3] Collison J. Osteoporosis: teriparatide preferable for fracture prevention. Nat Rev Rheumatol 2018;14:4.
[4] Simpson AH, Mills L, Noble B. The role of growth factors and related agents in accelerating fracture healing. J Bone Jt Surg Br Vol 2006;88:701–5.
[5] Lieberman JR, Daluiski A, Einhorn TA. The role of growth factors in the repair of bone. J Bone Jt Surg Am Vol 2002;84:1032–44.
[6] Féron JM, Mauprivez R. Féron Fracture repair: general aspects and influence of osteoporosis and anti-osteoporosis treatment. Injury 2016;47(Suppl 1):S10–4.
[7] Segredo-Morales E, García-García P, Reyes R, Pérez-Herrero E, Delgado A, Évora C. Bone regeneration in osteoporosis by delivery BMP-2 and PRGF from tetronic-alginate composite thermogel. Int J Pharm 2018;543:160–8.
[8] Yang P, Lv S, Wang Y, Peng Y, Ye Z, Xia Z, et al. Preservation of type H vessels and osteoblasts by enhanced preosteoclast platelet-derived growth factor type BB attenuates glucocorticoid-induced osteoporosis in growing mice. Bone 2018;114:1–13.
[9] McAlinden A, Im GI. MicroRNAs in orthopaedic research: disease associations, potential therapeutic applications, and perspectives. J Orthop Res 2018;36:33–51.
[10] Liang H, Gong F, Zhang S, Zhang CY, Zen K, Chen X. The origin, function, and diagnostic potential of extracellular microRNAs in human body fluids. Wiley Interdiscip Rev RNA 2014;5:285–300.
[11] Hanna Taipaleenmäki. Regulation of bone metabolism by microRNAs. Curr Osteoporos Rep 2018;16:1–12.
[12] Mei Y, Bian C, Li J, Du Z, Zhou H, Yang Z, et al. miR-21 modulates the ERK-MAPK signaling pathway by regulating SPRY2 expression during human mesenchymal stem cell differentiation. J Cell Biochem 2013;114:1374–84.
[13] Zhao Z, Li X, Zou D, Lian Y, Tian S, Dou Z. Expression of microRNA-21 in osteoporotic patients and its involvement in the regulation of osteogenic differentiation. Exp Ther Med 2019;17:709–14.
[14] Poynton AR, Lane JM. Safety profile for the clinical use of bone morphogenetic proteins in the spine. Spine 2002;27:S40–8.
[15] Luginbuehl V, Meinel L, Merkle HP, Gander B. Localized delivery of growth factors for bone repair. Eur J Pharm Biopharm 2004;58:197–208.
[16] Kurakhmaeva KB, Voronina TA, Kapica IG, Kreuter J, Nerobkova LN, Seredenin SB, et al. Antiparkinsonian effect of nerve growth factor adsorbed on polybutylcyanoacrylate nanoparticles coated with polysorbate-80. Bull Exp Biol Med 2008;145:259–62.
[17] Liu C, Wen J, Meng Y, Zhang K, Zhu J, Ren Y, et al. Efficient delivery of therapeutic miRNA nanocapsules for tumor suppression. Adv. Mater 2015;27:292–7.
[18] Li H, Wang Z, Fu Q, Zhang J. Plasma miRNA levels correlate with sensitivity to bone mineral density in postmenopausal osteoporosis patients. Biomarkers 2014;19:553–6.
[19] Hak DJ. The biology of fracture healing in osteoporosis and in the presence of anti-osteoporotic drugs. Injury 2018;49:1461–5.
[20] Hesse E, Neuerburg C, Kammerlander C, Stumpf U, Stange R, Böcker W. Influence of specific osteoporosis drugs on fracture healing. Unfallchirurg 2019;122:506–11.
[21] Armstrong DJ. Comment on: patients' preferences for anti-osteoporosis drug treatment: a cross-European discrete choice experiment. Rheumatology 2018;57:583–4.
[22] Paccou J, Cortet B. Bisphosphonate drug holidays in postmenopausal osteoporosis: effect on clinical fracture risk. Response to comments by Bredemeier. Osteoporos Int 2018;29:521.
[23] Wu DM, Zhang YT, Lu J, Zheng YL. Effects of microRNA-129 and its target gene c-Fos on proliferation and apoptosis of hippocampal neurons in rats with epilepsy via the MAPK signaling pathway. J Cell Physiol 2018;233:6632–43.
[24] Tokar T, Pastrello C, Rossos AEM, Abovsky M, Hauschild AC, Tsay M, et al. mirDIP 4.1-integrative database of human microRNA target predictions. Nucleic Acids Res 2018;46:D360–70.
[25] Huang J, Meng Y, Liu Y, Chen Y, Yang H, Chen D, et al. MicroRNA-320a regulates the osteogenic differentiation of human bone marrow-derived mesenchymal stem cells by targeting HOXA10. Cell Physiol Biochem 2016;38:40–8.
[26] Meng YB, Li X, Li ZY, Zhao J, Yuan XB, Ren Y, et al. microRNA-21 promotes osteogenic differentiation of mesenchymal stem cells by the PI3K/β-catenin pathway. J Orthop Res 2015;33:957–64.
[27] Zarecki P, Hackl M, Grillari J, Debono M, Eastell R. Serum microRNAs as novel biomarkers for osteoporotic vertebral fractures. Bone 2020;130:115105.
[28] Koevska V, Nikolikj-Dimitrova E, Mitrevska B, Gjeracaroska-Savevska C, Gocevska M, Kalcovska B. Effect of exercises on quality of life in patients with postmenopausal osteoporosis-randomized trial. Open Access Maced J Med Sci 2019;7:1160–5.
[29] Cheung WH, Miclau T, Chow SK, Yang FF, Alt V. Fracture healing in osteoporotic bone. Injury 2016;47:S21–6.
[30] Wong RM, Thormann U, Choy MH, Chim YN, Li MC, Wang JY, et al. A metaphyseal fracture rat model for mechanistic studies of osteoporotic bone healing. Eur Cell Mater 2019;37:420–30.
[31] Kolios L, Schumann J, Sehmisch S, Rack T, Tezval M, Seidlova-Wuttke D, et al. Effects of black cohosh (Cimicifuga racemosa) and estrogen on metaphyseal fracture healing in the early stage of osteoporosis in ovariectomized rats. Planta Med 2010;76:850–7.